RSC Chemical Biology

ROYAL SOCIETY OF CHEMISTRY

PAPER

View Article Online
View Journal | View Issue

Cite this: *RSC Chem. Biol.*, 2024, 5, 141

An AIE-based monofunctional Pt(II) complex for photodynamic therapy through synergism of necroptosis–ferroptosis†

Xiaoxue Zheng,‡[a] Minglun Liu,‡[a] Yanping Wu,[a] Yuncong Chen, *[ab] Weijiang He *[a] and Zijian Guo *[ab]

Received 30th June 2023,
Accepted 31st October 2023

DOI: 10.1039/d3cb00113j

rsc.li/rsc-chembio

Side effects and drug resistance are among the major problems of platinum-based anticancer chemotherapies. Photodynamic therapy could show improved tumor targeting ability and better anticancer effect by region-selective light irradiation. Here, we report an aggregation-induced emission (AIE)-based monofunctional Pt(II) complex (TTC-Pt), which shows enhanced singlet oxygen production by introduction of a Pt atom to elevate the intersystem crossing (ISC) rate. Moreover, TTC-Pt exhibits decent capacity of inhibition on tumor cell growth upon light irradiation, with negligible dark toxicity compared to the commonly used chemodrug cisplatin. Mechanistic study suggests that TTC-Pt enters HeLa cells *via* the endocytosis pathway and locates mainly in lysosomes, causing FSP1 down-regulation and intracellular lipid peroxidation accumulation under irradiation, finally leading to ferroptosis and necroptosis. The synergistic dual cell death pathways could help to kill apoptosis-resistant tumor cells. Therefore, TTC-Pt could serve as a potent antitumor photosensitizer, which overcomes the drug resistance with minimum side effects.

Introduction

Cancer is one of the biggest threats to human health.[1] Traditional cancer treatments such as surgery, chemotherapy and radiotherapy have to face problems including toxic side effects and drug resistance. Photodynamic therapy (PDT) exhibits the advantages of non-invasiveness, accuracy and effectiveness with minimal side effects and has attracted much attention.[2–4] The photosensitizers (PSs) after illumination will be excited from the ground state to the singlet excited state, transition to the triple excited state *via* an intersystem crossing (ISC) process, and generate reactive oxygen species (ROS).[5–7] Singlet oxygen ($^1O_2$) is one of the commonly generated ROS through the type II PDT process. It could easily react with biological molecules including unsaturated lipids and α-amino acids, disrupting intracellular balance and thus killing cancer cells.[8–12] Therefore, increasing $^1O_2$ yield is one of the effective ways to improve the efficacy of PDT.

To achieve a high yield of $^1O_2$, a common method is improving the rate constant of ISC (k_{ISC}).[13,14] There are usually two ways, one is to enhance intramolecular charge-transfer (ICT) states, and as a result, reduce the energy level difference between singlet and triplet states (ΔE_{ST}).[15–17] The other one is to improve the spin–orbit coupling (SOC) effect by introducing heavy atoms such as Pt, Ir, Ru and I, *etc.*[18–20] However, this way can potentially lead to increased dark toxicity, causing damage to normal cells.[21,22] Therefore, it is highly demanded to introduce appropriate heavy atoms into PSs to increase the $^1O_2$ yield while minimizing its toxic side effects. On the other hand, traditional PSs usually suffer from aggregation cause quenching of ROS generation due to the enhanced nonradiative decay rate.[23,24] In this regard, PSs with aggregation-induced emission (AIE) characteristics are beneficial to increase the $^1O_2$ generation yield by effective suppression of nonradiative decay and elevated population on the excited triplet state through the numerous ISC channels in the aggregation state.[25–27]

Some tumor cells show an altered signaling pathway to avoid apoptosis. Therefore, developing PSs that could kill tumor cells through other cell death pathways other than apoptosis is favorable to overcome the apoptosis-resistant tumor cells. Ferroptosis, a new iron-dependent form of non-apoptotic cell death pathway, has attracted a lot of attention because of its potential for effective cancer treatment.[28] In particular, cancer cells are resistant to apoptosis and

[a] *State Key Laboratory of Coordination Chemistry, School of Chemistry and Chemical Engineering, Chemistry and Biomedicine Innovation Center (ChemBIC), Nanjing University, Nanjing 210023, China. E-mail: chenyc@nju.edu.cn, heweij69@nju.edu.cn, zguo@nju.edu.cn*

[b] *Nanchuang (Jiangsu) Institute of Chemistry and Health, Nanjing 210000, China*

† Electronic supplementary information (ESI) available: Fig. S1–S10, Table S1 and all the experimental methods. See DOI: https://doi.org/10.1039/d3cb00113j

‡ These authors contributed equally.

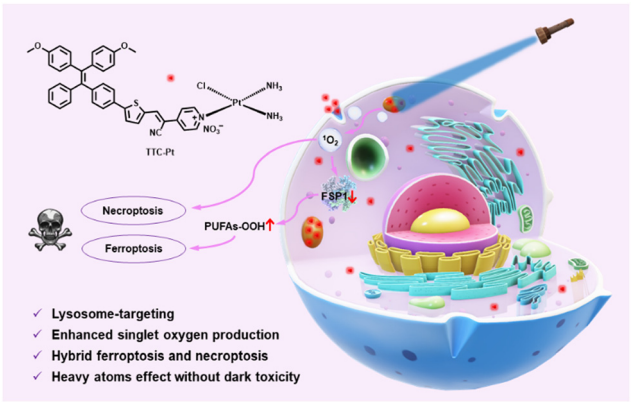

Scheme 1 An AIE-based monofunctional Pt(II) complex for photodynamic therapy through synergism of necroptosis–ferroptosis.

chemotherapeutics, and the characteristics of high proliferation of cancer cells lead to very active lipid metabolism and iron metabolism, laying the foundation for effective tumor elimination by ferroptosis.[29] At least three pathways have been identified to mediate ferroptosis: Xc^-/GSH/GPX4,[30] ACSL4/LPCAT3/ALOXs[31,32] and FSP1-CoQ10-NAD(P)H.[33,34] Most of the currently available ferroptosis inducers are based on the GPX4 pathway, while there are only a few reports on ferroptosis inducing PSs through other pathways.

In this contribution, we present a new AIE-based Pt(II) complex (TTC-Pt), which demonstrates efficient $^1O_2$ generation capacity, with a decomposition rate of ABDA (9,10-anthracenediyl-bis(methylene)dimalonic acid, a singlet oxygen indicator) up to 133.5 nmol per minute (Scheme 1). The AIE-active ligand TTC shows a donor–π–acceptor (D–π–A) structure, and a much lower $^1O_2$ generation rate.[35–37] The introduction of a Pt atom increases both the SOC effect and intramolecular charge transfer process, resulting in significantly elevated ROS generation capacity and the potential of image-guided PDT.[38] Interestingly, the introduction of heavy atom Pt did not increase the cellular dark toxicity of TTC-Pt. TTC-Pt enters HeLa cells *via* the endocytosis pathway and is located mainly in lysosomes, leading to down-regulation of FSP1 (ferroptosis suppressor protein 1) and accumulation of intracellular lipid peroxidation after irradiation, inducing ferroptosis and necroptosis. This study provides a powerful strategy for the development of high-performance PSs, which could help overcome both drug resistance and side effects.

Results and discussion

Molecular design and synthesis

AIE-based PSs with D–π–A structure can help to separate the distributions of the highest occupied molecular orbital (HOMO) and the lowest unoccupied molecular orbital (LUMO), which will further promote the k_{ISC} and thus favor the $^1O_2$ generation ability. TTC-Pt (Fig. 1a) was designed with a tetraphenyl (TPE) derivative as the electron-donating group (EDG), thiophene groups as π bridges and a cyano-pyridine moiety as an electron-withdrawing group (EWG)[39] to achieve better separation of HOMO–LUMO and reduce ΔE_{S-T} to promote the ISC process.[40] In addition, the introduction of cisplatin through coordination reaction, due to the heavy atom effect, would enlarge the spin–orbit coupling constant (ξ) between singlet and triplet states,[13] thereby improving ROS generation compared to the original AIE donor. The synthetic methods of PSs are shown in Scheme S1 (ESI†). All the compounds were fully characterized (Fig. S1–S5, ESI†).

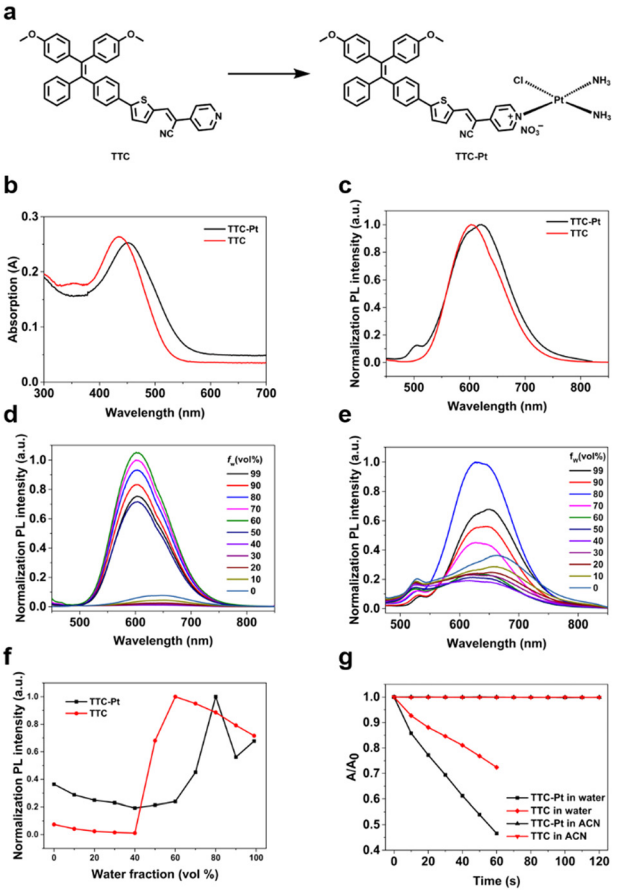

Fig. 1 (a) Chemical structures of TTC and TTC-Pt. (b) Absorption and (c) emission spectra of TTC and TTC-Pt (10 μM) were measured in water (containing 1% DMSO, v/v). Emission spectra of the AIEgens (10 μM) including (d) TTC and (e) TTC-Pt in the mixed solvents of DMSO and water with different water fractions (f_w). (f) Emission intensity plot of TTC-Pt and TTC in different f_w of the solvent mixture. (g) The decomposition rates of ABDA in the presence of TTC-Pt under illumination in different solvents (A_0 and A represent the absorption of ABDA before and after irradiation, respectively).

Photophysical characterization

The UV-vis and photoluminescence (PL) spectra of the AIE luminogens (AIEgens) in water were recorded in Fig. 1b and c. For the ligand TTC, it shows a maximum absorption peak at 434 nm and an emission at 603 nm, with a Stokes shift of 169 nm in aqueous solution. For TTC-Pt, it exhibits a red-shifted maximum absorption compared to TTC at 451 nm and a near-infrared (NIR) emission at 650 nm. Due to the Stokes shift

being nearly 200 nm, it is favorable for bioimaging because of the minimized interference between excitation and emission,[41] and thus it helps to improve the image-guided therapy. Using tris(2,2′-bipyridyl)dichlororuthenium(II) as a reference, the fluorescence quantum yields (QYs) of TTC and TTC-Pt were determined to be 11.45% and 2.9% in water (with 1% DMSO, v/v), and to be 0.46% and 0.6% in acetonitrile, respectively (Table S1, ESI†).

Fig. 1d and f show the PL spectra of TTC in the mixed solution with varied water fractions. In pure DMSO, TTC had almost no emission, but when the water fraction increases to 60%, the fluorescence intensity reaches the maximum with a nearly 50 nm blueshift. Even if the water fraction increases to 99%, it still has bright emission, revealing the AIE feature. In agreement with TTC, as the water fraction rises, the emission intensity of TTC-Pt was increased, and it reached the maximum when the water fraction was 80%, with the blue-shift of the emission maxima from around 664 to 651 nm (Fig. 1e and f). In addition, the transmission electron microscopy (TEM) and dynamic laser scattering (DLS) data also confirmed the irregular aggregation of AIEgens in aqueous solution (Fig. S6, ESI†). And they have decent stability in water (Fig. S7–S9, ESI†).

To measure the performance of TTC and TTC-Pt as PSs *in vitro*, their ability to produce $^1O_2$ was determined. With ABDA as the $^1O_2$ indicator, under irradiation at 450 nm, the absorbance of ABDA showed almost no change within 2 min in the presence of TTC or TTC-Pt in acetonitrile (Fig. S10, ESI†), suggesting poor $^1O_2$ generation capability in the molecular state even though acetonitrile can dissolve more O_2.[42] However, in water (contains 1% DMSO), it decreased sharply for 60 s under the same irradiation conditions (Fig. 1g and Fig. S11, ESI†), indicating that TTC and TTC-Pt possessed good $^1O_2$ production ability in the aggregation state. It is found that the indicator decomposition rate of TTC-Pt is 1.9 and 5.4-fold higher than that of TTC and Rose Bengal (RB), respectively, suggesting that the combination of cisplatin and the AIE moiety successfully improved the $^1O_2$ generation rate, in good agreement with expectations. In addition, respectively using dihydrorhodamine 123 (DHR123) and hydroxyphenyl fluorescein (HPF) as probes for $O_2^{\bullet-}$ and $^{\bullet}OH$, both TTC and TTC-Pt could increase the fluorescence intensity of the related probes with time (Fig. S12 and S13, ESI†), indicating that the two AIEgens should produce type I ROS and have the potential to overcome tumor hypoxia.

Cell uptake and subcellular accumulation

Cellular uptake is the basis of drug imaging and drug efficacy. HeLa cells were selected to monitor TTC-Pt and TTC drug uptake and intracellular location *via* confocal laser scanning microscopy (CLSM) in real time. As shown in Fig. S14 (ESI†), HeLa cells incubated with TTC-Pt can be clearly visualized after 1 h of incubation, while TTC only has weak fluorescence that is not visible to the naked eye under the same conditions. The fluorescence intensity of TTC-Pt did not change significantly after about 4 h, indicating that the uptake may have reached equilibrium, as TTC was about 6 h. This may be due to the introduction of positive charge, and TTC-Pt is more easily taken up by cells.[40] In addition, we also determined the Pt levels in HeLa cells incubated with TTC-Pt and CDDP, respectively, by ICP-MS. It was found that the former contained seven times more platinum than the latter (Fig. S14d, ESI†), which may be due to the introduction of fat-soluble groups that increased the uptake of drugs by cells. To further explore the way AIEgens

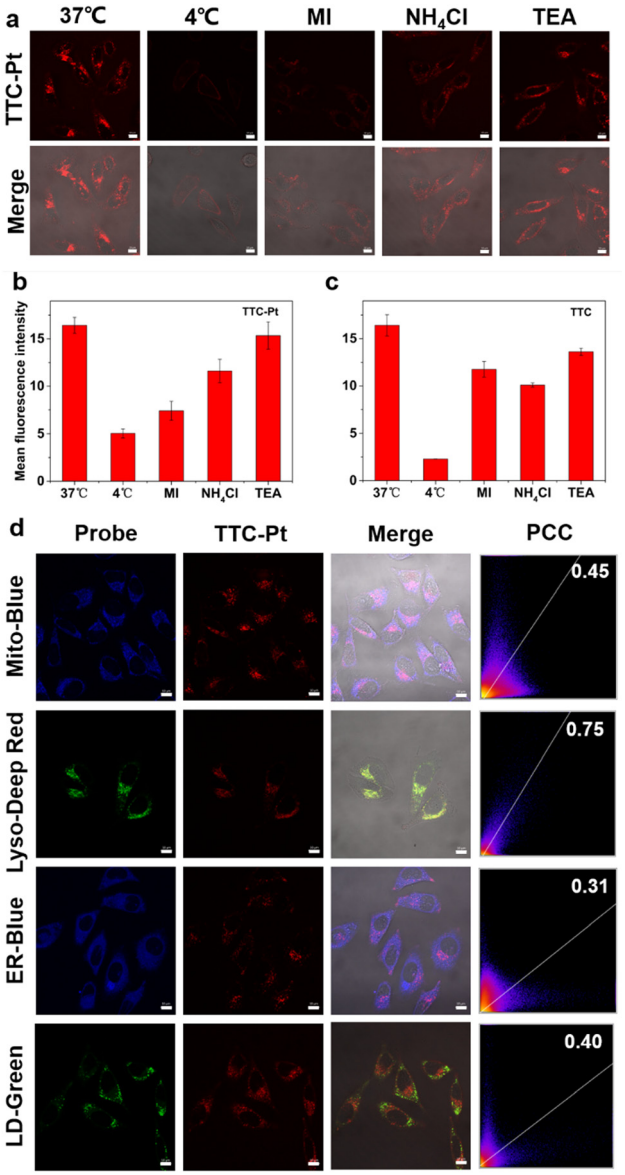

Fig. 2 (a) CLSM images of HeLa cells incubated with TTC-Pt (1 μM) in different conditions. The cells were pre-incubated with different inhibitors for 1 h or at different temperatures. Excitation: 488 nm; scanning channel: 600–700 nm; scale bar: 10 μm. MI: metabolic inhibitors, 2-deoxy-D-glucose (50 mM) and oligomycin (5 μM); NH_4Cl (50 mM); TEA: triethylamine (1 mM). (b) Fluorescence intensity change of cells in (a). (c) Fluorescence intensity change of cells with TTC and different endocytosis inhibitors including MI, NH_4Cl and TEA. (d) CLSM of HeLa cells stained with various commercial probes (Mito-Blue: 410–480 nm, λ_{ex}, 405 nm; Lyso-Deep Red: 650–680 nm, λ_{ex}, 633 nm; ER-Blue: 455–520 nm, λ_{ex}, 405 nm; LD-Green: 495–535 nm, λ_{ex}, 488 nm) and TTC-Pt (1 μM, 600–700 nm, λ_{ex}, 488 nm). Scale bar: 10 μm.

enter cells, the AIEgens were co-incubated with various cell uptake inhibitors. As shown in Fig. 2a and b, at low temperature (4 °C, which can inhibit transmembrane protein), MI (metabolic inhibitor) or NH_4Cl (endocytosis inhibitor), respectively, the intracellular fluorescence intensity of TTC-Pt decreased, suggesting that TTC-Pt entered cells mainly in the form of the energy-dependent transmembrane endocytosis pathway.[43]

Through the images of CLSM taken during cell uptake, both TTC-Pt and TTC successfully crossed the cell membrane and reached the cytoplasm. To further confirm the specific location of AIEgens within the cells, the subcellular distribution of TTC-Pt and TTC was achieved by co-incubation with various subcellular commercial dyes by CLSM (Fig. 2d and Fig. S16, ESI†). The Pearson's correlation coefficient (PCC) of the overlay fluorescence images between TTC-Pt and various dyes were 0.45 for Mito-Blue, 0.75 for Lyso-Deep Red, 0.31 for ER-Blue and 0.40 for LD-Green, respectively, indicating that TTC-Pt was mainly localized in lysosomes after entering cells. In addition, it has been reported that drugs entering cells through the endocytosis pathway are easy to accumulate in the lysosome, because the lysosome is the end point of endocytosis.[44] This also supports the lysosomal targeting ability of TTC-Pt. TTC shows no obvious organelle targeting (Fig. 2c and Fig. S15, S16, ESI†).

ROS generation and cytotoxicity of PSs against HeLa cells

The excellent $^1O_2$ generation capability and nice lysosomal targeting ability of TTC-Pt indicates that it could be considered as a good PS for cancer therapy. The ROS generation ability *in situ* was assessed by examining the fluorescence intensity of 2′,7′-dichlorofluorescin diacetate (DCFH-DA). As shown in Fig. 3a and b, HeLa cells incubated with TTC-Pt or TTC showed strong green fluorescence under light irradiation, while almost no fluorescence was observed in the dark or co-incubated with CDDP. Subsequently, the PDT effects of AIEgens were assessed by 3-(4,5-dimethylthiazol-2-yl)-2,5-diphenyltetrazolium bromide (MTT) assay. The half-maximal inhibitory concentrations (IC_{50}) to HeLa cells were measured to be 0.34 ± 0.05 μM for TTC-Pt, while that of TTC is over 64 μM. This indicated that the introduction of a Pt atom had indeed improved the phototoxicity of the drug, thus enhancing the effect of PDT. TTC-Pt and TTC showed no obvious cytotoxicity under dark conditions, and the cell viability was more than 80% when the drug concentration reached 64 μM (Fig. 3c and d and Table 1). Unlike the commonly enhanced dark toxicity by heavy atom introduction,[45] co-incubation of ligand TTC and CDDP led to significantly reduced dark toxicity (>64 μM) compared to that treated with CDDP alone (17.4 μM), and increased light toxicity (13.68 μM) compared to TTC alone (>64 μM). In addition, it was found that the Pt levels in the HeLa cells were reduced in the presence of TTC, indicating that TTC may inhibit the uptake of cisplatin and thus reduce the toxicity of cisplatin in the dark (Fig. S17, ESI†). The conversion from difunctional CDDP to monofunctional Pt(II) complex TTC-Pt could explain the reduced dark toxicity and increased light toxicity.

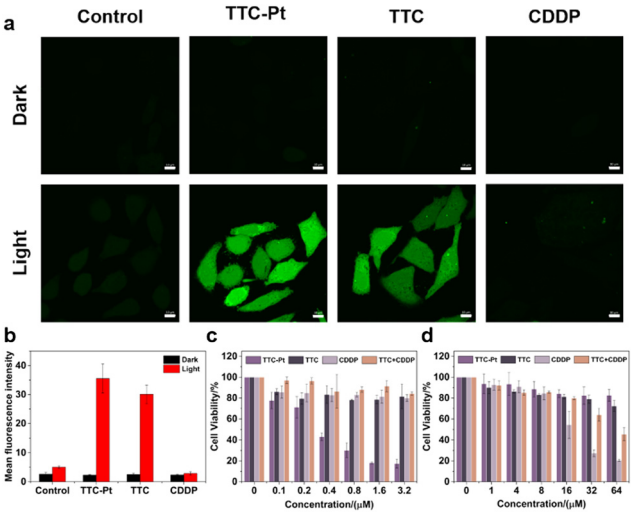

Fig. 3 Cytotoxicity of AIEgens against HeLa cells. (a) Confocal image of HeLa cells incubated with TTC (0.5 μM), TTC-Pt (0.5 μM), CDDP (0.5 μM) and DCFH-DA under irradiation (450 nm, 100 mW cm^{-2}, 1 min). Excitation: 488 nm. Scanning channel: 500–550 nm. Scale bar: 10 μm. (b) Fluorescence intensity change of DCFH stained cells in (a). Cell viabilities of cells after being incubated with different concentrations of TTC-Pt, TTC, CDDP and TTC + CDDP (c) with 450 nm laser irradiation at 100 mW cm^{-2} for 2 min and (d) in the dark (n = 3 biologically independent experiments).

Table 1 IC_{50} values of TTC-Pt, TTC, CDDP and TTC + CDDP against HeLa cells

Compounds	Irradiation[a] [μM]	Dark[b] [μM]
TTC-Pt	0.34 ± 0.05	>64.00
TTC	>64.00	>64.00
CDDP	25.28 ± 1.32	17.40 ± 3.42
TTC + CDDP	13.68 ± 1.99	>64.00

[a] 450 nm laser irradiation at 100 mW cm^{-2} for 2 min. [b] In the dark (n = 3 biologically independent experiments).

Cell death mode investigation

Cell death mechanisms initiated by the PSs usually show three main pathways including apoptosis, necroptosis and autophagy.[46] To elucidate the cell death pathways by this PDT process, we measured the viability of cells incubated with various cell death blockers and TTC-Pt. As shown in Fig. 4a, compared to the control co-incubated without any cell death inhibitor, there was no significant change of HeLa cell viability in the apoptosis inhibitor (z-VAD-fmk) group and the autophagy (3-methyladenine, 3-MA) group, while the cell viability was greatly improved after the addition of ferroptosis inhibitor (ferrostatin-1, Fer-1) or necroptosis inhibitor (necrostatin-1, Nec-1), indicating that necroptosis and ferroptosis were the main cell death modes induced by TTC-Pt after illumination. The dual cell death pathway caused by TTC-Pt is favorable to overcome apoptosis resistance tumor cells.

Ferroptosis induced by TTC-Pt

Lipid peroxide accumulation is the key characteristic of ferroptosis, which is caused by the free radical chain reaction that

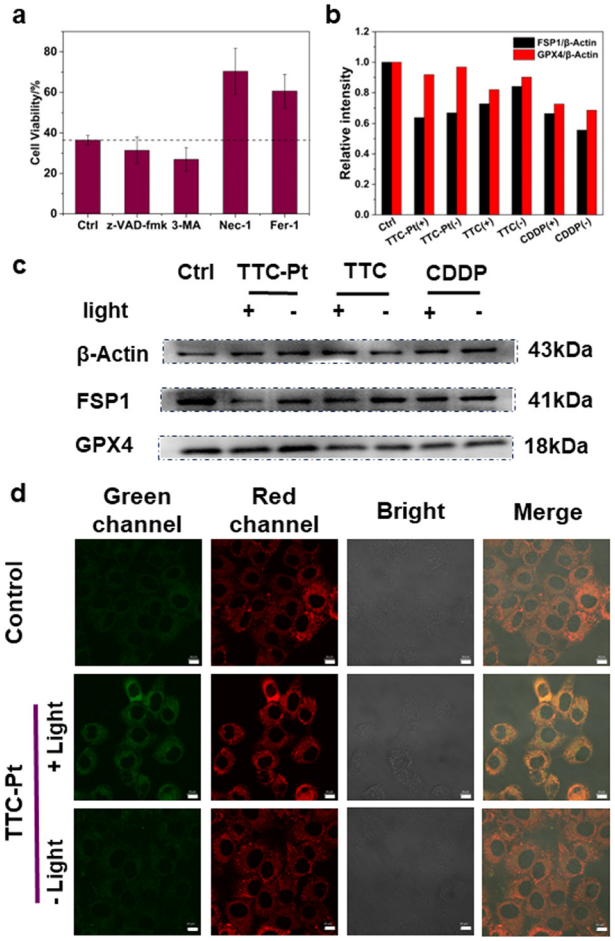

Fig. 4 Cell death mode investigation by PDT. (a) Cell viabilities of HeLa cells determined with TTC-Pt (0.8 μM) and different blockers. Before co-incubation with TTC-Pt, z-VAD-fmk (50 μM), 3-methyladenine (100 μM), necrostatin-1 (50 μM) and ferrostatin-1 (50 μM) were added for 1 h. For all tests, photoirradiation (450 nm, 100 mW cm^{-2}, 2 min) was imposed after 5 h of TTC-Pt addition. (b) The quantification of the blots for comparison in (c). (c) Expression of FSP1 and GPX4 in HeLa cells incubated with TTC-Pt, TTC or CDDP (1 μM) under or without light irradiation (100 mW cm^{-2}, 5 min). (d) CLSM images of HeLa cells incubated with TTC-Pt (1 μM) *via* C11-BODIPY staining, and photoirradiation (450 nm, 100 mW cm^{-2}, 2 min) was given after the staining. Scanning channels: 500–530 nm, λ_{ex}, 488 nm (green channel); 580–600 nm, λ_{ex}, 543 nm (red channel). Scale bar: 10 μm.

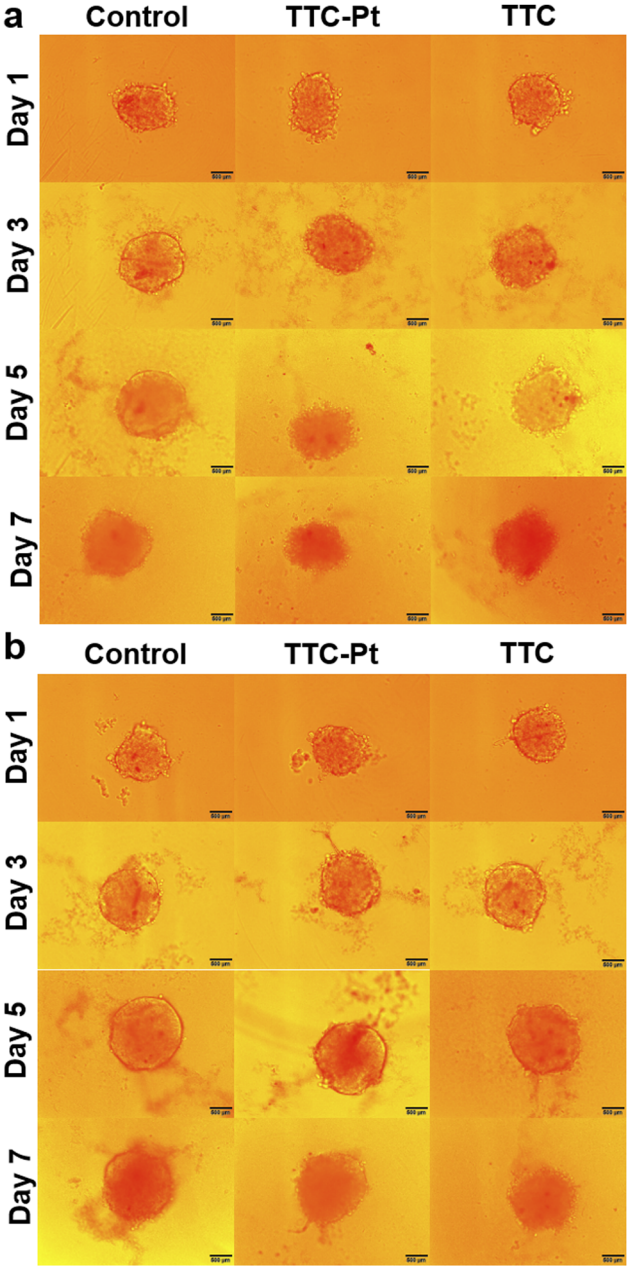

Fig. 5 Microscope images of HeLa MCSs. MCSs were incubated with 5 μM TTC and TTC-Pt (a) with or (b) without photoirradiation (450 nm, 127 mW cm^{-2}, 2 min). The day 1 images were taken before illumination, and then illumination was performed and images were taken every two days. Scale bar: 500 μm.

starts the autocatalytic autoxidation by abstracting a hydrogen atom from the bis-allylic position of polyunsaturated fatty acid (PUFA).[47] Fer-1 is a radical-trapping antioxidant that resists ferroptosis by scavenging ferrous oxide produced by lipid hydrogen peroxide and alkoxy radicals produced by other rearrangement products.[48] Therefore, in order to verify that ferroptosis was indeed induced by TTC-Pt *via* photoirradiation, we monitored the lipid peroxidation taking C11-BODIPY as a lipid peroxide probe.[49] Confocal imaging showed enhanced fluorescence of the green channels in HeLa cells incubated with TTC-Pt after irradiation, implying the lipid peroxide accumulation (Fig. 4d).

The system Xc-glutathione (GSH)-glutathione peroxidase 4 (GPX4) pathway is the most commonly reported ferroptosis prevention system, compared to other antioxidant systems, such as the ferroptosis inhibitory protein 1 (FSP1)-coenzyme Q10 (CoQ10) pathway.[50] To study the exact pathway that leads to ferroptosis, the expressions of key proteins GPX4 and FSP1 were investigated by western blot. As shown in Fig. 4b and c, the expression of FSP1 in HeLa cells incubated with TTC-Pt after irradiation was significantly down-regulated, while the expression of GPX4 all did not change obviously. What's more, it is reported that ubiquinol generated by FSP1 acts as an endogenous functional equivalent of the described small-molecule lipophilic radical scavengers Fer-1 inhibiting ferroptosis.[51] It

is inferred that ROS produced by TTC-Pt *via* irradiation could lead to the expression of FSP1 downregulation, triggering a series of REDOX imbalances that lead to ferroptosis in HeLa cells.

PDT effects in 3D multicellular spheroids (MCSs)

3D MCSs are microscale and spherical cell clusters formed by self-assembly. They are excellent models for tumors with central hypoxia due to the restriction on oxygen transmission.[52,53] The MCSs of HeLa cells were cultured with TTC-Pt or TTC, the medium was changed a half every two days, and photoirradiation (127 mW cm^{-2}, 2 min) was performed 24 h after medium change. MCSs cultured without AIEgens increased significantly in volume after 7 days whether with photoirradiation or not (Fig. 5a and b). Contrarily, the growth of MCSs cultured with AIEgens was obviously inhibited after light irradiation, especially with TTC-Pt, while in the dark, the volume was consistent with the control. The ability of AIEgens to inhibit the MCS growth after illumination suggested that they have the potential of anti-solid tumor. In particular, TTC-Pt has stronger inhibition ability than TTC, indicating that the synergistic necroptosis–ferroptosis is more favorable to anti-tumor activity for PDT.

Conclusions

In summary, we designed and synthesized a monofunctional Pt(II) complex based PS (TTC-Pt), which demonstrated attractive features such as aggregation enhanced ROS generation, high phototoxicity and low dark toxicity. TTC-Pt mainly localized in the lysosomes of HeLa cells, and could cause necroptosis and ferroptosis after illumination, and this synergistic effect could help eliminate apoptosis-resistant tumor cells. Moreover, the drug was able to cause ferroptosis through down-regulating the expression of FSP1, which is different from the conventional GPX4 pathway. This work provides new tools for effective and precise tumor treatment to overcome challenges faced by chemotherapy.

Author contributions

XZ and ML contributed to the work equally. XZ, ML, YC, WH and ZG designed the study. XZ and ML synthesized probes and performed the spectroscopic and cellular experiments; XZ and YW performed the experiments of western blots; XZ, ML and YC co-wrote the manuscript; ML, YC and YW revised the manuscript. All authors have read and given approval to the final version of the manuscript.

Conflicts of interest

There are no conflicts to declare.

Acknowledgements

The work was under financial support from the National Natural Science Foundation of China (Grants 22293050, 91953201, 92153303, 21977044, 22122701, 22377050, 21907050), the Natural Science Foundation of Jiangsu Province (BK20202004) and the Excellent Research Program of Nanjing University (ZYJH004).

Notes and references

1 W. Cao, H. D. Chen, Y. W. Yu, N. Li and W. Q. Chen, *Chin. Med. J.*, 2021, **134**, 783–791.
2 D. Cui, J. G. Huang, X. Zhen, J. C. Li, Y. Y. Jiang and K. Y. Pu, *Angew. Chem., Int. Ed.*, 2019, **58**, 5920–5924.
3 X. Y. Deng, Z. W. Shao and Y. L. Zhao, *Adv. Sci.*, 2021, **8**, 200254.
4 R. Wang, X. S. Li and J. Yoon, *ACS Appl. Mater. Interfaces*, 2021, **13**, 19543–19571.
5 X. Z. Zhao, J. P. Liu, J. L. Fan, H. Chao and X. J. Peng, *Chem. Soc. Rev.*, 2021, **50**, 4185–4219.
6 T. C. Pham, V. N. Nguyen, Y. Choi, S. Lee and J. Yoon, *Chem. Rev.*, 2021, **121**, 13454–13619.
7 D. D. Luo, K. A. Carter, D. Miranda and J. F. Lovell, *Adv. Sci.*, 2017, **4**, 1600106.
8 J. H. Correia, J. A. Rodrigues, S. Pimenta, T. Dong and Z. C. Yang, *Pharmaceutics*, 2021, **13**, 1332.
9 X. S. Li, S. Kolemen, J. Yoon and E. U. Akkaya, *Adv. Funct. Mater.*, 2017, **27**, 1604053.
10 U. Chilakamarthi and L. Giribabu, *Chem. Rec.*, 2017, **17**, 775–802.
11 Z. J. Zhang, M. M. Kang, H. Tan, N. Song, M. Li, P. H. Xiao, D. Y. Yan, L. P. Zhang, D. Wang and B. Z. Tang, *Chem. Soc. Rev.*, 2022, **51**, 1983–2030.
12 Y. P. Wu, S. M. Li, Y. C. Chen, W. J. He and Z. J. Guo, *Chem. Sci.*, 2022, **13**, 5085–5106.
13 K. K. Wen, H. Tan, Q. Peng, H. Chen, H. Ma, L. Wang, A. D. Peng, Q. Q. Shi, X. D. Cai and H. Huang, *Adv. Mater.*, 2022, **34**, 2108146.
14 B. M. Luby, C. D. Walsh and G. Zheng, *Angew. Chem., Int. Ed.*, 2019, **58**, 2558–2569.
15 L. Q. Li, C. Shao, T. Liu, Z. C. Chao, H. L. Chen, F. Xiao, H. M. He, Z. X. Wei, Y. L. Zhu, H. Wang, X. D. Zhang, Y. T. Wen, B. Yang, F. He and L. L. Tian, *Adv. Mater.*, 2020, **32**, 2003471.
16 S. D. Xu, Y. Y. Yuan, X. L. Cai, C. J. Zhang, F. Hu, J. Liang, G. X. Zhang, D. Q. Zhang and B. Liu, *Chem. Sci.*, 2015, **6**, 5824–5830.
17 F. Hu, S. D. Xu and B. Liu, *Adv. Mater.*, 2018, **30**, 1801350.
18 J. Z. Zhao, W. H. Wu, J. F. Sun and S. Guo, *Chem. Soc. Rev.*, 2013, **42**, 5323–5351.
19 W. J. Zhao, Z. K. He and B. Z. Tang, *Nat. Rev. Mater.*, 2020, **5**, 869–885.
20 A. M. Potocny, J. J. Teesdale, A. Marangoz, G. P. A. Yap and J. Rosenthal, *Inorg. Chem.*, 2019, **58**, 5042–5050.
21 A. Turksoy, D. Yildiz and E. U. Akkaya, *Coord. Chem. Rev.*, 2019, **379**, 47–64.
22 V. N. Nguyen, S. Qi, S. Kim, N. Kwon, G. Kim, Y. Yim, S. Park and J. Yoon, *J. Am. Chem. Soc.*, 2019, **141**, 16243–16248.

23 G. Yang, J. S. Ni, Y. X. Li, M. L. Zha, Y. Tu and K. Li, *Angew. Chem., Int. Ed.*, 2021, **60**, 5386–5393.
24 G. Xu, C. W. Li, C. Chi, L. Y. Wu, Y. Y. Sun, J. Zhao, X. H. Xia and S. H. Gou, *Nat. Commun.*, 2022, **13**, 13.
25 R. Y. Zhang, X. L. Huang, C. Chen, R. T. K. Kwok, J. W. Y. Lam and B. Z. Tang, *Mater. Sci. Eng., R*, 2021, **146**, 100649.
26 Y. C. Chen, J. W. Y. Lam, R. T. K. Kwok, B. Liu and B. Z. Tang, *Mater. Horiz.*, 2019, **6**, 428–433.
27 L. Yang, X. J. Wang, G. Z. Zhang, X. F. Chen, G. Q. Zhang and J. Jiang, *Nanoscale*, 2016, **8**, 17422–17426.
28 Z. X. Xie, H. D. Hou, D. Luo, R. An, Y. P. Zhao and C. Qiu, *Inflammation*, 2021, **44**, 35–47.
29 Y. H. Lv, M. Y. Wu, Z. Wang and J. Q. Wang, *Cell Biol. Toxicol.*, 2023, **39**, 827–851.
30 S. J. Dixon, D. Patel, M. Welsch, R. Skouta, E. Lee, M. Hayano, A. G. Thomas, C. Gleason, N. Tatonetti, B. S. Slusher and B. R. Stockwell, *eLife*, 2014, **3**, e02523.
31 S. Doll, B. Proneth, Y. Y. Tyurina, E. Panzilius, S. Kobayashi, I. IngoId, M. Irmler, J. Beckers, M. Aichler, A. Walch, H. Prokisch, D. Trumbach, G. W. Mao, F. Qu, H. Bayir, J. Fullekrug, C. H. Scheel, W. Wurst, J. A. Schick, V. E. Kagan, J. P. F. Angeli and M. Conrad, *Nat. Chem. Biol.*, 2017, **13**, 91–98.
32 X. Chen, R. Kang, G. Kroemer and D. L. Tang, *Nat. Rev. Clin. Oncol.*, 2021, **18**, 280–296.
33 K. Bersuker, J. M. Hendricks, Z. P. Li, L. Magtanong, B. Ford, P. H. Tang, M. A. Roberts, B. Q. Tong, T. J. Maimone, R. Zoncu, M. C. Bassik, D. K. Nomura, S. J. Dixon and J. A. Olzmann, *Nature*, 2019, **575**, 688–692.
34 S. Doll, F. P. Freitas, R. Shah, M. Aldrovandi, M. C. da Silva, I. Ingold, A. G. Grocin, T. N. X. da Silva, E. Panzilius, C. H. Scheel, A. Mourao, K. Buday, M. Sato, J. Wanninger, T. Vignane, V. Mohana, M. Rehberg, A. Flatley, A. Schepers, A. Kurz, D. White, M. Sauer, M. Sattler, E. W. Tate, W. Schmitz, A. Schulze, V. O'Donnell, B. Proneth, G. M. Popowicz, D. A. Pratt, J. P. F. Angeli and M. Conrad, *Nature*, 2019, **575**, 693–698.
35 W. B. Wu, D. Mao, F. Hu, S. D. Xu, C. Chen, C. J. Zhang, X. M. Cheng, Y. Y. Yuan, D. Ding, D. L. Kong and B. Liu, *Adv. Mater.*, 2017, **29**, 1700548.
36 A. D. Shao, Y. S. Xie, S. J. Zhu, Z. Q. Guo, S. Q. Zhu, J. Guo, P. Shi, T. D. James, H. Tian and W. H. Zhu, *Angew. Chem., Int. Ed.*, 2015, **54**, 7275–7280.
37 Y. Y. Li, Q. C. Peng, S. J. Li, Y. C. Cai, B. Zhang, K. Sun, J. B. Ma, C. P. Yang, H. W. Hou, H. F. Su and K. Li, *Sens. Actuators, B*, 2019, **301**, 127139.
38 Y. Y. Yuan, C. J. Zhang, M. Gao, R. Y. Zhang, B. Z. Tang and B. Liu, *Angew. Chem., Int. Ed.*, 2015, **54**, 1780–1786.
39 M. L. Liu, Y. C. Chen, Y. Guo, H. Yuan, T. X. Cui, S. K. Yao, S. X. Jin, H. H. Fan, C. J. Wang, R. Xie, W. J. He and Z. J. Guo, *Nat. Commun.*, 2022, **13**, 2179.
40 B. Guo, M. Wu, Q. Shi, T. J. Dai, S. D. Xu, J. W. Jiang and B. Liu, *Chem. Mater.*, 2020, **32**, 4681–4691.
41 Z. Zheng, T. F. Zhang, H. X. Liu, Y. C. Chen, R. T. K. Kwok, C. Ma, P. F. Zhang, H. H. Y. Sung, I. D. Williams, J. W. Y. Lam, K. S. Wong and B. Z. Tang, *ACS Nano*, 2018, **12**, 8145–8159.
42 Q. Li, C. Batchelor-McAuley, N. S. Lawrence, R. S. Hartshorne and R. G. Compton, *J. Electroanal. Chem.*, 2013, **688**, 328–335.
43 H. Yuan, Z. Han, Y. C. Chen, F. Qi, H. B. Fang, Z. J. Guo, S. R. Zhang and W. J. He, *Angew. Chem., Int. Ed.*, 2021, **60**, 8174–8181.
44 K. Q. Qiu, Y. Chen, T. W. Rees, L. N. Ji and H. Chao, *Coord. Chem. Rev.*, 2019, **378**, 66–86.
45 S. J. Liu, H. K. Zhang, Y. Y. Li, J. K. Liu, L. L. Du, M. Chen, R. T. K. Kwok, J. W. Y. Lam, D. L. Phillips and B. Z. Tang, *Angew. Chem., Int. Ed.*, 2018, **57**, 15189–15193.
46 E. Buytaert, M. Dewaele and P. Agostinis, *Biochim. Biophys. Acta, Rev. Cancer*, 2007, **1776**, 86–107.
47 J. P. F. Angeli, R. Shah, D. A. Pratt and M. Conrad, *Trends Pharmacol. Sci.*, 2017, **38**, 489–498.
48 G. Miotto, M. Rossetto, M. L. Di Paolo, L. Orian, R. Venerando, A. Roveri, A. M. Vuckovic, V. B. Travain, M. Zaccarin, L. Zennaro, M. Maiorino, S. Toppo, F. Ursini and G. Cozza, *Redox Biol.*, 2020, **28**, 101328.
49 E. H. W. Pap, G. P. C. Drummen, V. J. Winter, T. W. A. Kooij, P. Rijken, K. W. A. Wirtz, J. A. F. Op den Kamp, W. J. Hage and J. A. Post, *FEBS Lett.*, 1999, **453**, 278–282.
50 M. Liu, X. Y. Kong, Y. Yao, X. A. Wang, W. Yang, H. Wu, S. Li, J. W. Ding and J. Yang, *Ann. Transl. Med.*, 2022, **10**, 368.
51 C. M. Bebber, F. Muller, L. P. Clemente, J. Weber and S. von Karstedt, *Cancers*, 2020, **12**, 164.
52 L. L. Sun, Y. Chen, S. Kuang, G. Y. Li, R. L. Guan, J. P. Liu, L. N. Ji and H. Chao, *Chem. – Eur. J.*, 2016, **22**, 8955–8965.
53 Y. Imamura, T. Mukohara, Y. Shimono, Y. Funakoshi, N. Chayahara, M. Toyoda, N. Kiyota, S. Takao, S. Kono, T. Nakatsura and H. Minami, *Oncol. Rep.*, 2015, **33**, 1837–1843.